

Influence of atmospheric plasma spraying process parameters on microstructure and properties of yttrium oxide coatings

J. J. Li^a, Y. F. Zhang^{a,*}, Q. Li^b, X.Y. Ran^c, Q. Hao^c, X. L. Guo^a

^a*School of Mechanical Engineering, Qilu University of Technology (Shandong Academy of Sciences), Jinan, Shandong, 250353, PR China*

^b*School of Material Science and Engineering, Qilu University of Technology (Shandong Academy of Sciences), Jinan, Shandong, 250353, PR China*

^c*Weihai Yinxing Prestressed Wire Products Co.,Ltd, Weihai, Shandong, 264200, PR China*

Y₂O₃ coatings were fabricated on using atmospheric plasma spraying (APS). The effects of different process parameters on the microstructure and properties of the coating were analyzed. The results show that the overall morphology of Y₂O₃ coatings are smooth at high spraying power, low spraying distance and low primary gas flow rate, which is consistent with the change trend of porosity and hardness. The minimum porosity of coating is about 1.4%. The roughness of coatings isn't sensitive to changes in parameters. Y₂O₃ coatings have excellent corrosion resistance. The smaller the porosity of Y₂O₃ coating, the better the corrosion resistance.

(Received June 22, 2023; Accepted January 2, 2024)

Keywords: Atmospheric plasma spraying, Y₂O₃ coating, Process parameters, Porosity

1. Introduction

As a ceramic coating, yttrium oxide coating can strengthen the corrosion resistance, wear resistance, thermal barrier and high temperature oxidation resistance of the metal substrate^[1, 2], thereby increasing the service life of the metal substrate and expanding the scope of application. The metal matrix materials protected by ceramic coating also possess excellent properties of metals, such as high strength, high plasticity, electrical conductivity, etc., as well as excellent properties such as corrosion resistance, stability, high temperature oxidation resistance and hard texture of ceramic materials in the coating, so the materials combined by coating and matrix are suitable for many fields^[3].

Plasma etching plays an essential role in semiconductor manufacturing to ensure that mask patterns are correctly replicated onto silicon wafers^[4]. Dry etching is the selective removal and retention of materials and areas on silicon wafers by plasma to fabricate highly integrated transistors^[5]. With the development of semiconductor technology, dry etching has gradually become a widely used technique in the fabrication of micro and micro and nano semiconductor

* Corresponding author: zhangyanfei@qlu.edu.cn

devices due to its high repetition rate, anisotropy, insensitivity to temperature, few particles in the environment, and non-selectivity^[6, 7]. However, during the production process, plasma can also cause erosion of the components inside the etching chamber, resulting in reduced device component life and higher maintenance costs. The material in the etching chamber is generally aluminum alloy, which is difficult to resist the erosion of high-energy plasma. Therefore, it is necessary to select a material as the etch-resistant coating.

Yttrium oxide coating, as a new corrosion resistant material, is widely used in semiconductor etching process chamber lining because of its resistance to high-power plasma^[8, 9]. Junya et al.^[10] found that the corrosion resistance of Y_2O_3 was 5 to 7 times that of Al_2O_3 , a commonly used corrosion resistant material at this stage. Compared with alumina, its chemical properties are very stable, and the reaction product YF_3 generated with commonly used CF-based etching gases has a low vapor pressure, which is difficult to disperse as particles and will not contaminate the wafer^[11]. At present, many research institutions at home and abroad have carried out studies on the preparation of high-purity yttrium oxide coatings and their properties by plasma spraying^[12-14]. Plasma spraying process parameters have an important impact on the performance of the coating, among them, the porosity plays an important role in the performance of many properties of the coating, so the high-purity yttrium oxide coating with better performance can be prepared by adjusting the process parameters. However, there are few studies on the influence of Y_2O_3 spraying process parameters on coating performance.

Therefore, in this paper, Y_2O_3 coatings were prepared using atmospheric plasma spraying technology under different process parameters, and the effects of the parameters on the micromorphology, porosity, hardness, surface roughness and corrosion resistance of Y_2O_3 coatings were investigated.

2. Experiment Procedures

2.1. Coating Deposition

Commercially available Y_2O_3 powder (15-53 μm , 99.95%, Oerlikon Metco) was used as the coating material, and its chemical composition was shown in Table 1. 304 steel samples with dimensions of 13 mm \times 10 mm \times 2 mm were used as the substrate material. Before plasma spraying, 304 steel substrates were ultrasonically cleaned and sandblasted. The purpose of sandblasting is to remove the surface impurities and increase the roughness of the coating surface by using 60# white corundum with compressed air pressure of 0.6-0.8 MPa. The bond coating material used nickel-clad aluminum composite powder (45-80 μm) produced by Jinzhou Jinjiang Spraying Material Co., Ltd. The bond coating was added to increase the bonding strength between the coating and substrate and prevent the coating from breaking and falling off during the cooling process. The atmospheric plasma spraying equipment used the ZB-80K spraying system of Beijing Aerospace Zhenbang Precision Machinery Co., Ltd., and the spraying gas adopted a combination of argon and hydrogen. The spraying parameters of the bond coating are listed in Table 2. Six groups of optimized process parameters were used to prepare Y_2O_3 coatings as shown in Table 2. The obtained coatings are referred to as S1, S2, S3, S4, S5 and S6 respectively. The entire coating process was carried out indoors to prevent excessive oxidation during the formation of the coating. After spraying, the samples were air-cooled to room temperature to prevent large internal stress between coatings. Samples were collected and further analysis was performed on its.

Table 1. Chemical composition of Y_2O_3 powder.

Fe	Na	Mg	Al	Si	K	Ca	Y_2O_3
5	3	3	10	10	10	10	balance

Table 2. Spraying process parameters of Ni-Al bond coating and Y_2O_3 coatings.

Parameters	S1	S2	S3	S4	S5	S6	Ni-Al
Voltage(V)	65	65	65	65	65	65	70
Current(A)	550	550	550	600	600	600	598
Primary gas flow(L/min)	32	32	38	38	38	31	34
Secondary gas flow(L/min)	2	2	2	2	2	2	3
Power feed rate(RPM)	4.7	4.7	4.7	6	6	6	6
Spray distance (mm)	130	100	100	100	110	100	150

2.2. Material Characterization

A scanning electron microscope (GeminiSEM 500, Carl Zeiss, Germany) was used to observe the surface and section of the sprayed powder and the coating, and its morphology and microstructure were analyzed. The composition and element distribution of the coating surface and cross section were analyzed by energy dispersion spectrometer. The X-ray diffraction (SmartlabSE, Rigaku, Japan) was measured to characterize the phase components using, which was operated at 40 kV and 100 mA using Cu - $K\alpha$ radiation with the scanning range of 10-80° and a scanning speed of 20 °/min. The surface roughness was measured by confocal laser scanning microscope (KC-XI000, KathMatic). The coating porosity was measured by Image-Pro-Plus analysis software using the cross section image obtained by SEM. A micro Vickers hardness tester (HXD-1000TMC) was used to measure the Vickers hardness of the Y_2O_3 coating with a test load of 0.98 N and a loading time of 15 s. The microhardness measurement was performed on a ground and polished cross-section of the coating, and the measurement was taken as an average of 5 points. The coatings were tested for corrosion in 3.5 wt% NaCl solution using an electrochemical workstation (CHI660E) at room temperature. A three-electrode system was used in the experiment: coatings and 304 steel were used as working electrodes with an exposed area of 1 cm², a saturated calomel electrode was used as a reference electrode, and a platinum sheet was used as an auxiliary electrode. First, the open-circuit potential (OCP) tests were performed for 3600S in order to obtain the steady state potential, and then dynamic potential polarization curves with a potential variation range of -0.5-1 V (vs OCP) were measured at a scan rate of 0.5 mV/s.

3. Results and Discussion

3.1. Powder Characteristics

Fig. 1 shows the particle size of Y_2O_3 powder, which is mainly between 20-30 μ m. The SEM images of Y_2O_3 powder are shown in Fig. 2. The powder is prepared by agglomeration

sintering process, which first forms the powder through agglomeration process and then sintering it to remove the adhesive, increase the cohesion strength of the particles and partially densify them^[15]. Most of the powder particles are regular in shape, spherical or ellipsoidal, as shown in Fig. 2 (a) and (b), but the structure is not dense, and even some particles have obvious depressions or local hollows, as shown in Fig. 2 (b). Enlarge the local area of the particles and find a large number of fine particles agglomerated together, as shown in Fig. 2 (c). The composition of the powder is uniform as shown in Fig. 2 (d). The powder prepared by agglomeration sintering method has the characteristics of high sphericity, good fluidity, and the improvement of loose packing density, which makes it easier to plasma spraying. Fig. 3 of the XRD pattern of Y_2O_3 powder shows that the powder contains only a single cubic phase of Y_2O_3 . In addition, the intensity and position of the diffraction peaks are consistent with the standard diffraction card (PDF#41-1105).

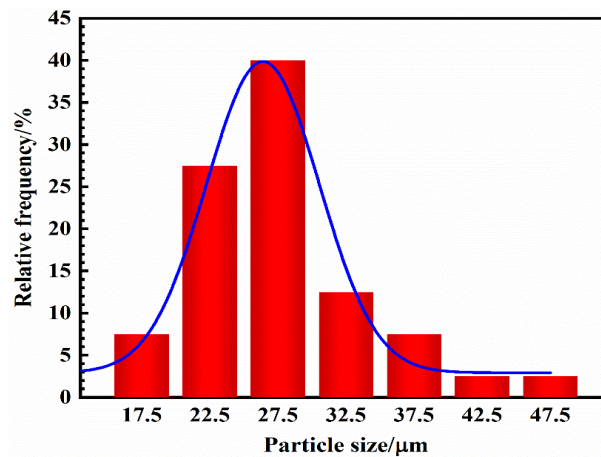


Fig. 1. Particle size of Y_2O_3 powder.

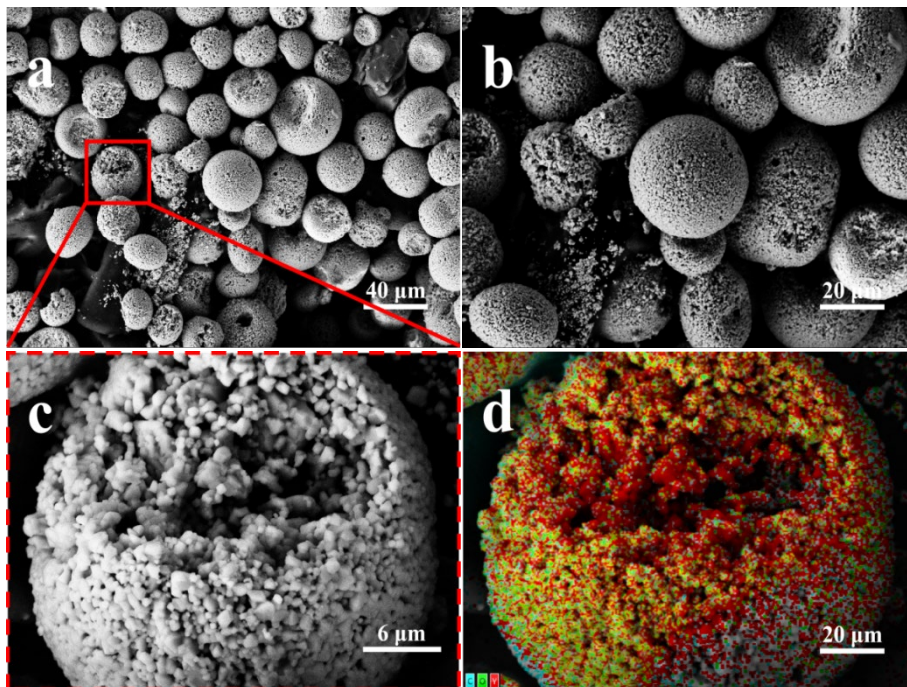


Fig. 2. (a), (b) and (c) SEM image of Y_2O_3 powder; (d) EDS analysis.

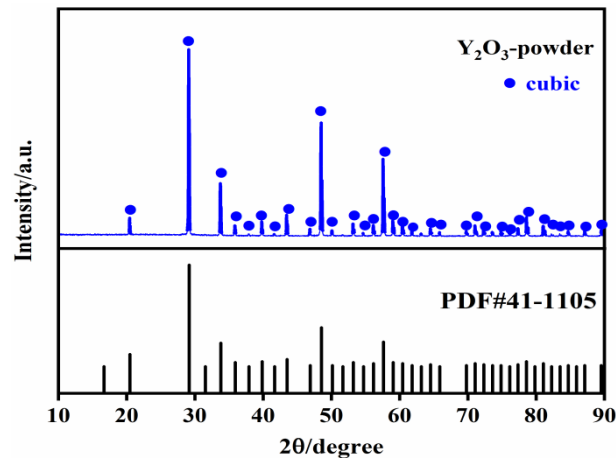


Fig. 3. XRD pattern of Y_2O_3 powder.

3.2. Coating characteristics

The phase composition of Y_2O_3 powder and coating has little change, and Y_2O_3 coating only contains a single cubic crystal phase, which is mainly related to the properties of the material itself. In addition, the diffraction peaks do not shift, indicating that the material does not undergo severe lattice expansion or contraction. Compared with the diffraction pattern of powder and coating in Fig. 4, it can be seen that the basic composition is basically the same before and after spraying, and the XRD diffraction peak of powder is higher than that of coating, mainly because spraying particles hit the surface of matrix material at high speed, plastic deformation occurs, and the grain is refined, which leads to the reduction of the diffraction peak intensity of coating. The broadening of the XRD peaks of the coating is mainly due to the fact that the powder particles tend to form smaller grain sizes during rapid solidification and cooling, resulting in the broadening of the XRD peaks of the Y_2O_3 coatings.

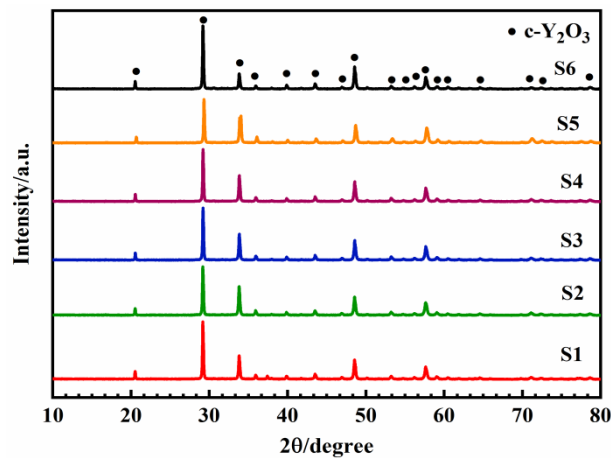


Fig. 4. XRD patterns of Y_2O_3 coatings.

The surface SEM images of Y_2O_3 coatings with different process parameters is shown in Fig. 5. There are different degrees of Pore, cracks, fully melted zone (FM) and partially melted zone (PM) on the surface of each group of samples. During the spraying process, the particles fully absorb heat while flying in the plasma flame zone and are completely melted before reaching the substrate, and are completely spread out when they hit the substrate, resulting in a smooth, flat and densely structured FM zone. The particles that do not sufficiently absorb heat remain solid at the core, although the surface melts into liquid state, and only a small area is spread out when they hit the substrate, resulting in a granular and raised PM zone.

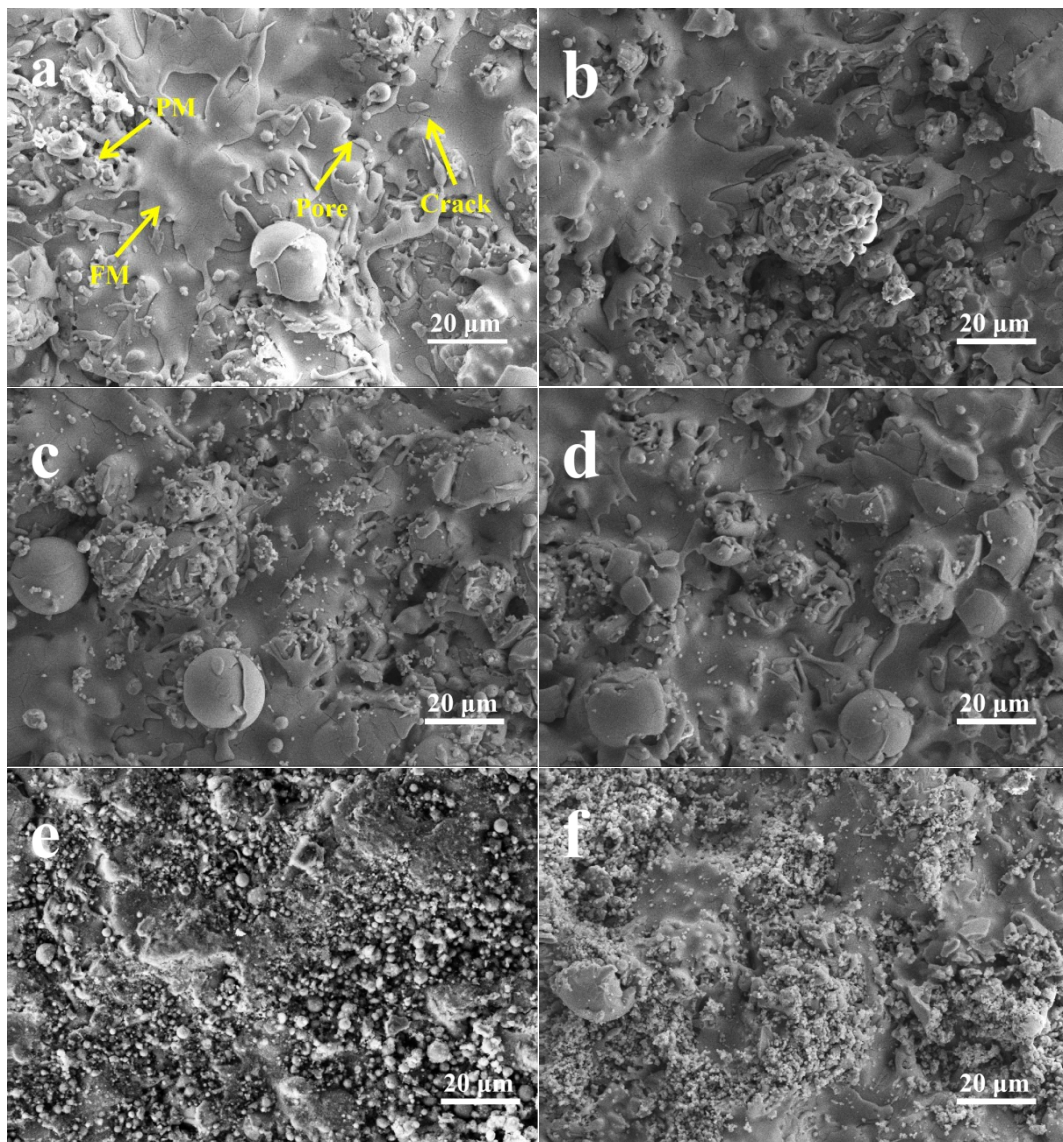


Fig. 5. Surface SEM images of Y_2O_3 coatings: (a) S1; (b) S2; (c) S3; (d) S4; (e) S5 and (f) S6.

The variable parameter of S1 and S2 is the spraying distance, which mainly affects the melting degree of powder. If the spraying distance is too close, the Y_2O_3 powder will reach the substrate surface without time to melt, so that the powder cannot be fully combined with the substrate surface, and the performance of coating is reduced. If the spraying distance is too far, the

limited flame flow energy will cause the melted powder to solidify again, so that the particles reaching the substrate surface will become unmelted particles, which will also increase the porosity of the coating and affect the performance of the coating. During the spraying process, it was found that when the spraying distance is 130 mm, there was a layer of floating end on the surface of the coating, which indicates that the spraying distance is too far will make the molten particles consume too much energy in the process of flight, so that when it reaches the surface of the substrate, the tamping effect played by the particles that reached the coating before is also reduced by a lot. Compared with S2, S3 increases the primary gas flow, which mainly affects the temperature and flow rate of Y_2O_3 powder in the plasma flame flow. S3 increases the primary gas flow rate leading to lower temperature and higher flow rate, and the Y_2O_3 powder stays in the plasma flame flow for too short a time and cannot be heated and melted sufficiently, which makes the unfused particles increase when reaching the substrate surface and affects the coating quality. Compared with S3, S4 increases the spraying power and powder feeding rate, the spraying power is mainly to control the temperature and energy of the plasma gun flame stream, properly increase the spraying power, the plasma flame stream temperature will also increase, so that the spraying powder particles melt more fully. In contrast to S4, the increased spraying distance of S5 leads to limited flame flow energy, which makes the melted powder solidify again, so that the particles that reach the substrate surface become unmelted particles. S6 reduces the main gas flow rate and the Y_2O_3 powder melting degree is increased.

Plasma coating is formed by a large number of sprayed particles extruded and piled up on the surface of the substrate. Its cross-sectional microstructure is generally parallel and uneven laminated structure, and there are pores and cracks, as shown in Fig. 6. These are typical characteristics of coatings prepared by atmospheric plasma spraying technology^[16, 17]. These pores can be roughly divided into two categories: one is the large (about a few microns) but the number of irregular pores is small; the other type of pores are small ($<1 \mu\text{m}$) but abundant and dispersed in the coating. The causes of the pores are complex, and the larger pores are caused by the incomplete flattening of some of the droplets during their contact with the collective and incomplete lap with the surrounding particles. The small circular voids are due to the fact that during the plasma spraying process, the high-speed jet gas and the ambient gas entering by volume suction are partially dissolved inside the molten particles, and the high-speed droplets are rapidly cooled after contact with the substrate, and part of the dissolved gas inside the coating does not have time to precipitate out^[18]. In addition, there are microscopic cracks in the coating, such as transverse cracks, which are perpendicular to the deposition direction and present a relatively uniform distribution. Cracks mainly exist between lamellar flakes and are related to the flattening and accumulation of molten particles. On the other hand, the longitudinal microcracks are approximately parallel to the deposition direction and are mainly associated with pores and other defects in the coating. The formation of longitudinal microcracks is caused by the rapid cooling of molten particles after impact on the substrate surface, during which a large amount of thermal stress is released.

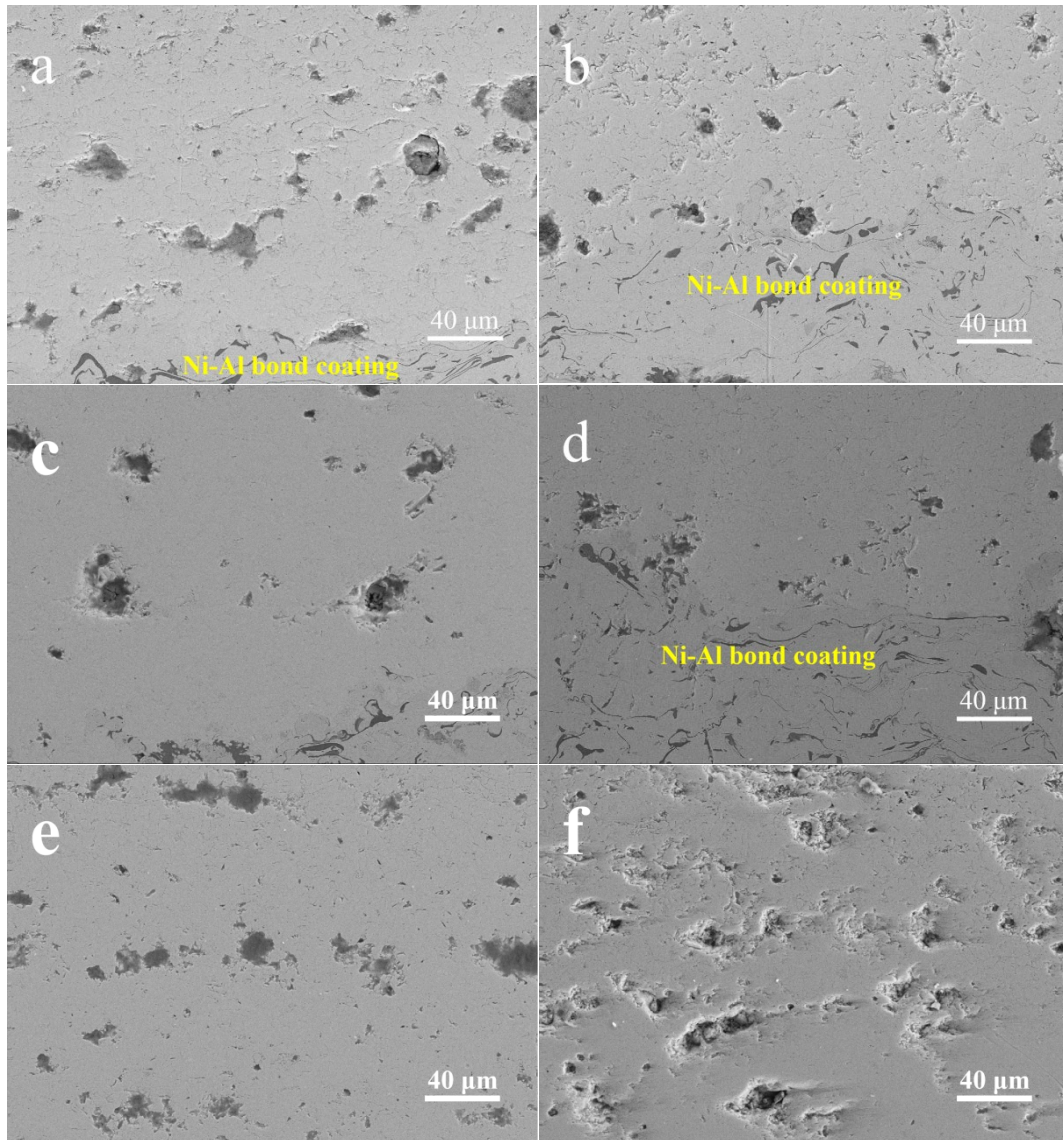


Fig. 6. Cross-sectional SEM images of the Y_2O_3 coatings: (a) S1; (b) S2; (c) S3; (d) S4; (e) S5 and (f) S6

Fig. 7 shows confocal microscopic images of the surface of the Y_2O_3 coating, using two-dimensional images to determine the height distribution. The wide range of height distribution indicates that the surface is not smooth. There is little change in the height difference between S1-S6. The surface roughness values of Y_2O_3 coating measured by CLSM are shown in Fig. 8. The roughness of S1-S6 is 3.84, 3.86, 3.18, 3.37, 2.98 and 3.64 μm , and the height varies from 69.45, 64.82, 58.60, 54.44, 57.66 and 73.01 μm , respectively. The surface roughness of the coating is not consistent with the preparation process, in other words, the coating roughness is not sensitive to the change of the preparation process parameters.

The cross-sectional images of the Y_2O_3 coatings obtained by SEM and the porosity of the coating measured by Image-Pro-Plus image analysis software is shown in Fig. 9. The lowest porosity is about 1.4 % for S2 and the highest is about 5.4 % for S5. As the spraying distance decreases, the porosity decreases. The increase of primary gas flow leads to the increase of porosity. The porosity decreases with the increase of spraying power. This result is consistent with the analysis of surface and cross section morphology of the coating. It has been shown^[19, 20] that the resistance to plasma erosion of

coatings of the same material and preparation method depends on the densities of the coatings themselves.

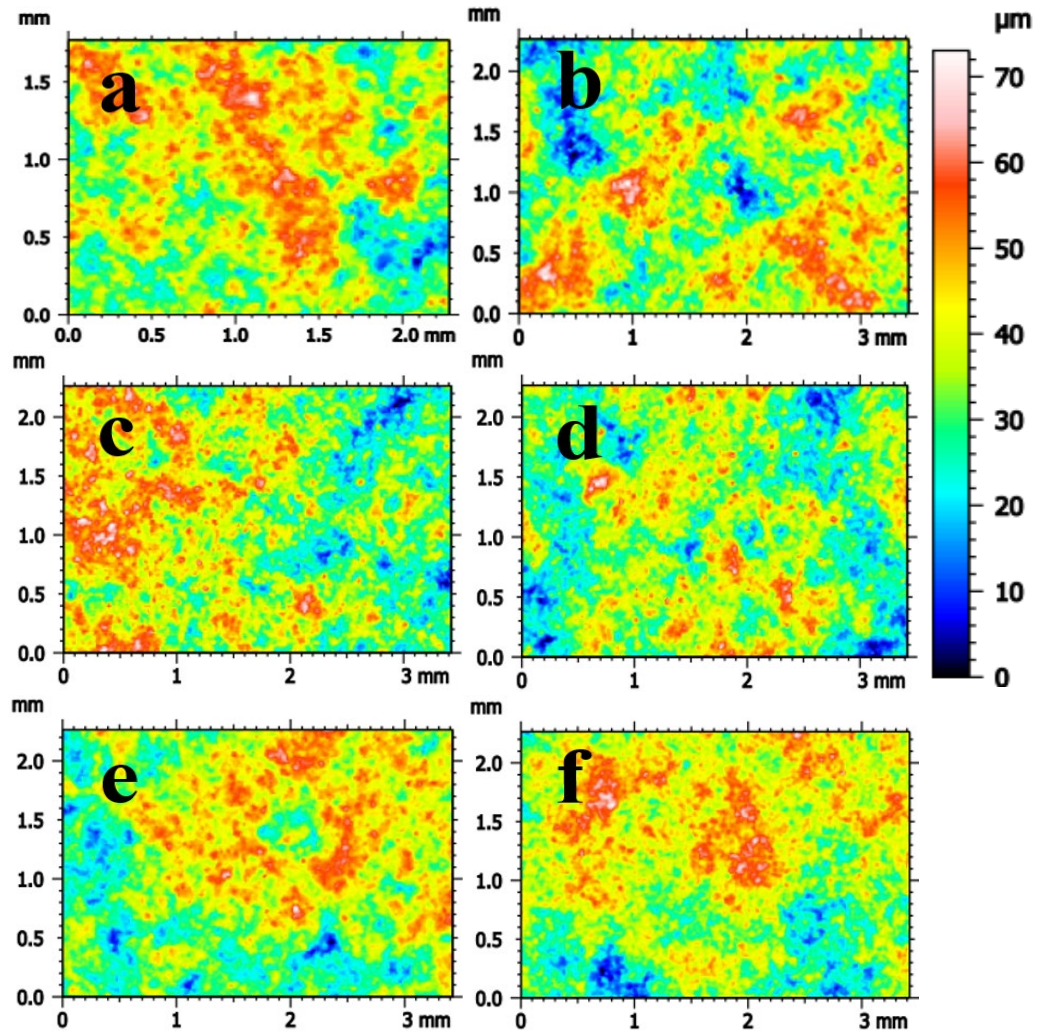


Fig. 7. Confocal microscope images of Y_2O_3 coatings: (a) S1; (b) S2; (c) S3; (d) S4; (e) S5 and (f) S6.

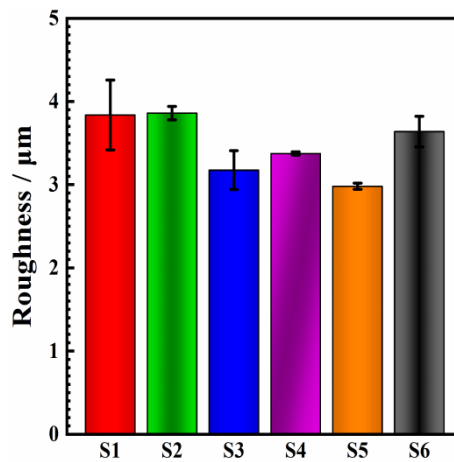


Fig. 8. Surface roughness of Y_2O_3 coatings.

The denser the coating structure, the slower the rate of its own loss in the plasma etching environment, thus achieving better protection of the substrate. In contrast, porosity has a direct effect on coating etch resistance^[21], as corrosion around pores is faster and easier than corrosion on dense surfaces. Samples with lower porosity exhibit superior etch resistance, which is attributed to the smaller exposed area of the low porosity sample surface in the plasma atmosphere. The Vickers hardness of the Y_2O_3 coating is shown in Figure 9, and the hardness of S1-S6 is 514.2 HV_{0.1}, 497.6 HV_{0.1}, 504.4 HV_{0.1}, 517.3 HV_{0.1} and 463.3 HV_{0.1} respectively. the variation pattern of the preparation process parameters on the hardness remains consistent with the porosity. The hardness of coatings prepared by APS is usually influenced by the porosity. The higher the porosity, the lower the hardness, as described in the following equation^[22]:

$$S = S_0 \exp(-bP) \quad (1)$$

where S , S_0 , b , and P denote the mechanical properties of the test material, the mechanical properties of the free porous material, the constant coefficient, and the porosity of the sample, respectively. Typically, as porosity increases, hardness decreases. However, the results of this experiment show that the hardness increases with the increase of porosity. This is because the percentage of pores exceeding 10 μm was reduced and the fraction of pores exceeding 10 μm significantly affected the hardness of the Y_2O_3 coating prepared by APS^[14].

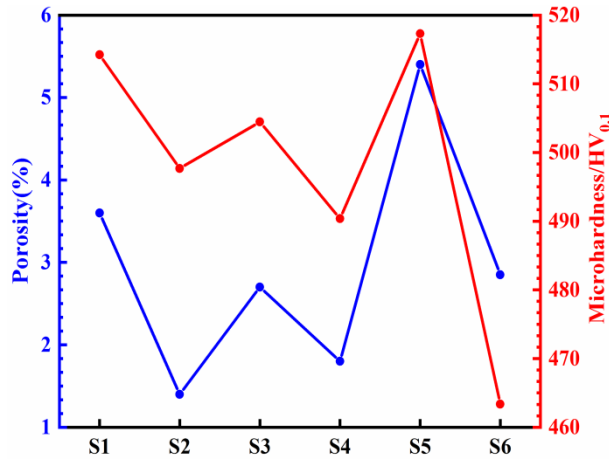


Fig. 9. Porosity and Vickers hardness of Y_2O_3 coatings.

Fig. 10 shows the potentiodynamic polarization curves of Y_2O_3 coatings and 304 steel in 3.5 wt% NaCl solution, and the fitted data were obtained by Tafel extrapolation as shown in Table 4. where β_a is the anodic Tafel slope; β_c is the cathodic Tafel slope; E_{corr} is the corrosion potential; i_{corr} is the corrosion current density; and R_p is the polarization resistance, which is defined as follows^[23]:

$$R_p = \frac{\beta_a \beta_c}{2.303 i_{corr} (\beta_a + \beta_c)} \quad (2)$$

The E_{corr} of S1-S6 and 304 steel is -0.655 , -0.532 , -0.560 , -0.548 , -0.773 , -0.575 and

-0.796 V, respectively. The E_{corr} reflects the corrosion tendency of the coating; the more positive the E_{corr} , the smaller the corrosion tendency. The E_{corr} of 304 steel was significantly lower than that of the coating, indicating that the Y_2O_3 coating played a protective role against corrosion. The i_{corr} is 3.16×10^{-9} , 5.01×10^{-10} , 1×10^{-9} , 7.94×10^{-10} , 5.01×10^{-9} , 1.58×10^{-9} and 1.58×10^{-8} $\text{A} \cdot \text{cm}^{-2}$, respectively. The i_{corr} of the coatings values are approximately 1/5, 1/31.5, 1/15.8, 1/19.8, 1/3.15, 1/10, respectively, of the substrate. The corresponding R_p is 2.07×10^8 , 3.02×10^9 , 1.53×10^9 , 1.54×10^9 , 8.6×10^7 , 8.5×10^8 and 6.9×10^7 $\Omega \cdot \text{cm}^2$, respectively. When determining the corrosion resistance of materials, i_{corr} is more important than E_{corr} [24], and corrosion current density is proportional to corrosion rate [25]. The lower the i_{corr} , the higher the R_p , and the better the corrosion resistance [26, 27]. Corrosion resistance in the order of $\text{S2} > \text{S4} > \text{S3} > \text{S6} > \text{S1} > \text{S5} > 304$ steel. This result is consistent with the porosity of the Y_2O_3 coating, where high porosity provides more corrosion pathways and degrades the coating quality. The lower the porosity, the better the corrosion resistance of the coating.

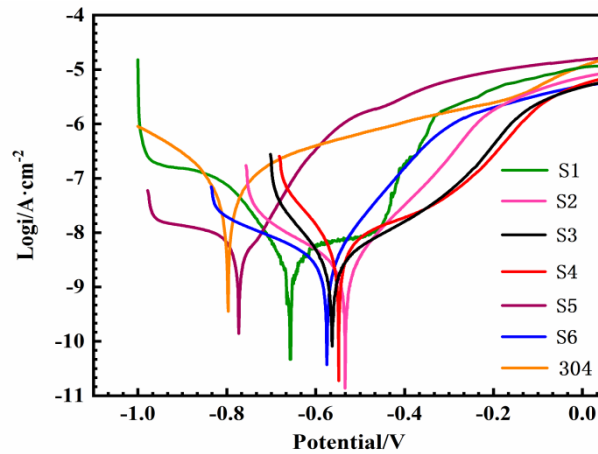


Fig. 10. Potentiodynamic polarization curves of Y_2O_3 coatings and 304 steel in 3.5 wt% NaCl solution.

Table 4. Fitting results of polarization curves.

Sample	β_a ($\text{V} \cdot \text{dec}^{-1}$)	$-\beta_c$ ($\text{V} \cdot \text{dec}^{-1}$)	E_{corr} (V)	i_{corr} ($\text{A} \cdot \text{cm}^{-2}$)	R_p ($\Omega \cdot \text{cm}^2$)
S1	1.75	10.95	-0.655	3.16×10^{-9}	2.07×10^8
S2	9.68	5.46	-0.532	5.01×10^{-10}	3.02×10^9
S3	5.16	11.13	-0.560	1×10^{-9}	1.53×10^9
S4	3.83	10.76	-0.548	7.94×10^{-10}	1.54×10^9
S5	16.57	2.25	-0.773	5.01×10^{-9}	8.6×10^7
S6	11.08	4.3	-0.575	1.58×10^{-9}	8.5×10^8
304	4.49	5.8	-0.796	1.58×10^{-8}	6.9×10^7

4. Conclusion

Y₂O₃ coatings with different process parameters were successfully prepared, and the effects of different process parameters on the organization and properties of the coatings were investigated in depth. High spraying power, low spraying distance and low main gas flow rate are more conducive to melting and binding of powder to substrate. The changes of process parameters have the same effect on the porosity and Vickers hardness of coating. The Y₂O₃ coating reduces the corrosion tendency, and the corrosion resistance of the coating is also consistent with the porosity. The greater the porosity of the coating, the easier it is for the corrosive medium to enter the substrate through the pores to cause corrosion reactions, and the corrosion resistance is poorer. It is found that when the spraying current is 65 A, the voltage is 600 V, the primary gas flow rate is 32 L/min, the secondary gas flow rate is 2 L/min, and the spraying distance is 100 mm, the coating has a stable cubic phase, smooth morphology, the smallest porosity and the best corrosion resistance.

Acknowledgements

The project was supported by Qilu University of Technology (Shandong Academy of Sciences) - Weihai City Industry-University-Research Collaborative Innovation Fund 2022CXY-03.

References

- [1] X. He, X. H. Yuan, H. Xu, P. Song, X. Yu, C. Li, T. H. Huang, Q. L. Li, K. Y. Lü, J. Feng, J. G. Lü and J. S. Lu, *Ceramics International* **45**(12), 14546 (2019); <http://doi.org/10.1016/j.ceramint.2019.04.171>
- [2] A. A. Abdel-Samad, A. M. M. El-Bahloul, E. Lugscheider and S. A. Rassoul, *Journal of Materials Science* **35**(12), 3127 (2000); <http://doi.org/10.1023/A:1004824104162>
- [3] L. J. Li, Y. D. He, D. R. Wang and R. D. Xue, *High Temperature Materials Processes* **4**(1), 85 (2005); <http://doi.org/doi:10.1515/HTMP.2005.24.1.85>
- [4] V. M. Donnelly and A. Kornblit, *Journal of Vacuum Science & Technology A: Vacuum, Surfaces, and Films* **31**(5), 050825 (2013); <http://doi.org/10.1116/1.4819316>
- [5] V. Lotito and T. Zambelli, *Advances in Colloid and Interface Science* **299**, 102538 (2022); <http://doi.org/10.1016/j.cis.2021.102538>
- [6] Y. S. Cho, G. R. Yi, J. H. Moon, D. C. Kim, B. J. Lee and S. M. Yang, *Journal of Colloid and Interface Science* **341**, 209 (2010); <http://doi.org/10.1016/j.jcis.2009.09.060>
- [7] L. L. Yan, K. Wang, J. S. Wu and L. Ye, *Journal of Physical Chemistry B* **110**(23), 11241 (2006); <http://doi.org/10.1021/jp057228z>.
- [8] H. K. Seok, E. Y. Choi, P. R. Cha, M. C. Son and B. L. Choi, *Surface and Coatings Technology* **205**(11), 3341 (2011); <http://doi.org/10.1016/j.surfcoat.2010.10.045>
- [9] G. F. Yang, P. Chen, Z. L. Wu, Z. G. Yu, H. Zhao, B. Liu, X. M. Hua, Z. L. Xie, X. Q. Xiu and P. Han, *Journal of Materials Science: Materials in Electronics* **23**(6), 1224 (2012); <http://doi.org/10.1007/s10854-011-0577-5>
- [10] J. Kitamura, H. Ibe, F. Yuasa and H. Mizuno, *Journal of Thermal Spray Technology* **17**(5-6), 878 (2008); <http://doi.org/10.1007/s11666-008-9285-y>
- [11] Y. C. Cao, L. Zhao, J. Luo, K. Wang, B. P. Zhang, H. Yokota, Y. Ito and J. F. Li, *Applied Surface Science* **366**, 304 (2016); <http://doi.org/10.1016/j.apsusc.2016.01.092>

- [12] J. Kitamura, H. Ibe, F. Yuasa and H. Mizuno, *Journal of Thermal Spray Technology* **17**(5), 878 (2008); <http://doi.org/10.1007/s11666-008-9285-y>
- [13] T. K. Lin, D. S. Wu, S. Y. Huang and W. K. Wang, *Japanese Journal of Applied Physics* **55**(12), 126201 (2016); <http://doi.org/10.7567/jjap.55.126201>
- [14] D. S. Lee, S. Yun, J. W. Han, M. Y. Song, Y. G. Kim, J. K. Lee, J. Choi, S. Chang, S. Hong and J. H. Kim, *Ceramics International* **47**(3), 3853 (2021); <http://doi.org/10.1016/j.ceramint.2020.09.246>
- [15] G. Bolelli, C. Lyphout, L. M. Berger, V. Testa, H. Myalska-Głowacka, P. Puddu, P. Sassatelli and L. Lusvarghi, *Wear* **512-513**, 3364 (2023); <http://doi.org/10.1016/j.wear.2022.204550>
- [16] F. Wang, G. N. Luo, J. J. Huang and Y. Liu, *Surface and Coatings Technology* **358**, 276 (2019); <http://doi.org/10.1016/j.surfcoat.2018.11.046>
- [17] X. Qiao, Y. M. Wang, W. X. Weng, B. L. Liu and Q. Li, *Ceramics International* **44**(17), 21564 (2018); <http://doi.org/10.1016/j.ceramint.2018.08.220>
- [18] A. Kulkarni, A. Vaidya, A. Goland, S. Sampath and H. Herman, *Materials Science and Engineering A* **A359**(1-2), 100 (2003); [http://doi.org/10.1016/s0921-5093\(03\)00342-3](http://doi.org/10.1016/s0921-5093(03)00342-3)
- [19] H. Kwon, Y. Kim, H. Park and C. Lee, *Surface and Coatings Technology* **374**, 493 (2019); <http://doi.org/10.1016/j.surfcoat.2019.05.052>
- [20] H. Ashizawa and K. Yoshida, *Ceramics International* **45**(17), 21162 (2019); <http://doi.org/10.1016/j.ceramint.2019.07.093>
- [21] R. Kreethi, Y. J. Hwang, H. Y. Lee, J. H. Park and K. A. Lee, *Surface and Coatings Technology* **454**, 129182 (2023); <http://doi.org/10.1016/j.surfcoat.2022.129182>
- [22] C. J. Li and A. Ohmori, *Journal of Thermal Spray Technology* **11**(3), 365 (2002); <http://doi.org/10.1361/105996302770348754>
- [23] W. Zhao and D. J. Kong, *Applied Surface Science* **481**, 161 (2019); <http://doi.org/10.1016/j.apsusc.2019.03.047>
- [24] X. L. Zhang, Z. H. Jiang, Z. P. Yao, Y. Song and Z. D. Wu, *Corrosion Science* **51**(3), 581 (2009); <http://doi.org/10.1016/j.corsci.2008.12.005>
- [25] A. A. Rodriguez, J. H. Tylczak, M. C. Gao, P. D. Jablonski, M. Detrois, M. Ziomek-Moroz and J. A. Hawk, *Advances in Materials Science and Engineering* **2018**, 1 (2018); <http://doi.org/10.1155/2018/3016304>
- [26] D. Jiang, H. Z. Cui, H. Chen, X. F. Zhao, G. L. Ma and X. J. Song, *Materials & Design* **210**, 110068 (2021); <http://doi.org/10.1016/j.matdes.2021.110068>
- [27] K. Rahmani, G. H. Majzoobi, H. Bakhtiari and A. Sadooghi, *Materials Chemistry and Physics* **271**, 124946 (2021); <http://doi.org/10.1016/j.matchemphys.2021.124946>